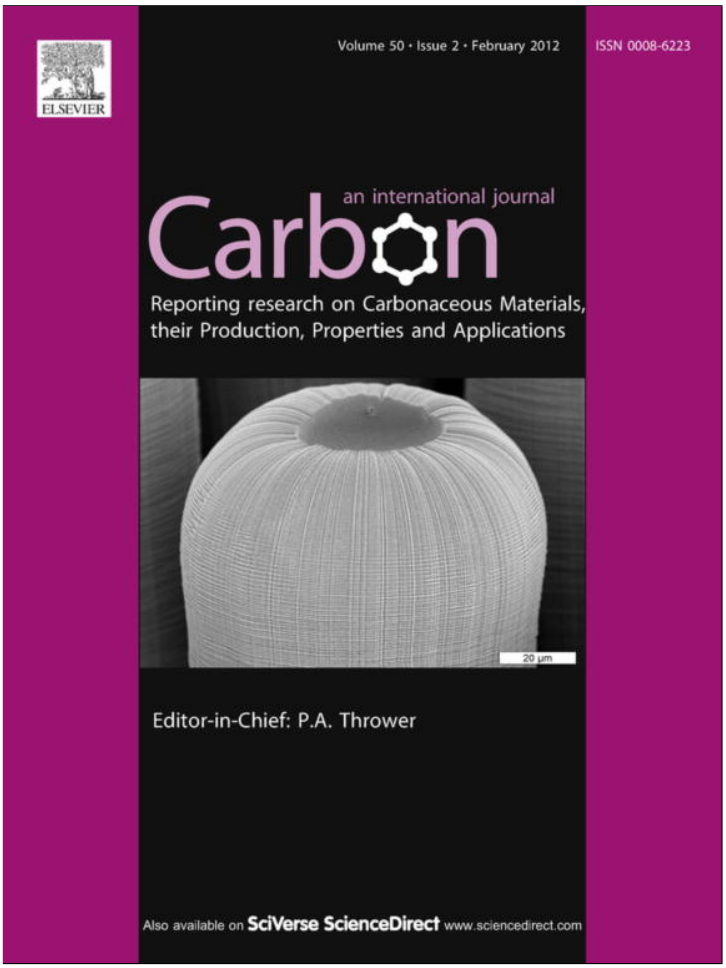

CARBON 50 (2012) 404–410

Available at www.sciencedirect.com

SciVerse ScienceDirect

journal homepage: www.elsevier.com/locate/carbon

Molecular dynamics simulation study of the growth of a rough amorphous carbon film by the grazing incidence of energetic carbon atoms

Minwoong Joe, Myoung-Woon Moon, Jungsoo Oh, Kyu-Hwan Lee, Kwang-Ryeol Lee *

Computational Science Center, Korea Institute of Science and Technology, P.O. Box 131, Cheongryang, Seoul 130-650, South Korea

ARTICLE INFO

Article history:
Received 26 June 2011
Accepted 26 August 2011
Available online 5 September 2011

ABSTRACT

The morphological evolution of an amorphous carbon film deposited by energetic carbon atoms of 75 eV with various angles of incidence was investigated by molecular dynamics simulation. Normal or near-normal incidence of carbon atoms resulted in a smooth surface of the deposited film. In contrast, a bump-like surface structure emerged and led to rough surfaces at grazing incidences, in agreement with the experiments. The bifurcated growth mode was explained by the impact-induced transport of atoms on the growing surface. The downhill transport of atoms on a sloping surface dominates at normal incidence, which suppresses the evolution of surface irregularities to form a rough surface. However, the dominance of uphill transport at a grazing incidence made the surface irregularities grow to a seed structure, which provided the shadowing effect during carbon deposition. This mechanism mediates initial seed formation and subsequent roughening together with shadowing effects under grazing incidence.

1. Introduction

Surface structure control of amorphous carbon (a-C) film is essential for various engineering applications. Due to their high surface area or porosity [1], amorphous carbon films with high surface area have potential applications in energy conversion and storage devices such as supercapacitors [2] or hydrogen storage devices [3]. A rough surface of amorphous carbon can be utilized in a controlled manner by glancing angle deposition (GLAD). This technique is based on thin film deposition at a high incidence angle (>60°) together with optional substrate rotation. Surface roughening or seeding behavior in the initial stage of a-C film growth, using energetic carbon atoms (40–70 eV) and grazing incidence angles (60–70°), has been experimentally reported in clear contrast with smooth surfaces under normal and near-normal incidences (0–30°) [4,5].

Many experimental works of GLAD show the significant role of the incidence angle on both growth orientation and film porosity; the higher the incidence angle the more tilted and porous the columnar structure [6,7]. By varying the geometry of deposition during film growth by, for instance, altering the in-plane beam direction or the rotating substrate or both, a variety of three-dimensional structures can be produced [8,9]. The evolution of the film structure is attributed to the shadowing effect and low diffusivity of deposited atoms [10,11]. Pre-deposited atoms can block subsequent deposition in the shadowed region under grazing incidence conditions. The local variation of beam flux together with limited surface diffusion can lead to a porous film with columnar structures tilted toward the ion source. Although the shadowing effect provides a coherent explanation of the rough film growth with a preexisting seed surface structure, it is still ambiguous how the seed surface structure evolves from a nominally

* *Corresponding author:* Fax: +82 2 958 5509.
E-mail address: krlee@kist.re.kr (K.-R. Lee).
0008-6223/$ - see front matter © 2011 Elsevier Ltd. All rights reserved.
doi:10.1016/j.carbon.2011.08.053

smooth surface to provide the shadowing effect. In the initial stage of growth, the surface irregularities are ill-defined due to atomic scale fluctuation of the surface or randomly-arranged hillocks. Nonetheless, for prolonged depositions under a grazing incidence, a seed structure is evolved on the initially smooth surface and then develops into a columnar structure. The seed formation mechanism at a grazing incidence is thus essential to complete the understanding of the rough surface evolution during glancing angle deposition.

Molecular dynamics (MD) simulation of the initial seed formation would enable one to understand the mechanism of the rough surface evolution in atomic scale. Although a series of MD studies of amorphous carbon deposition has focused on the atomic structure of the film as a function of incidence energy of carbon ion [12–18], only a few works are available on the surface structure evolution. Surface smoothening under normal or near-normal incidence condition was investigated in the light of atomic displacements: ion-induced downhill transport [19] or transverse-migration-induced relaxation [20]. However, the effect of grazing incidence angle on surface roughening has yet to be clarified in the atomic scale.

In this paper, the onset of surface roughening from atomic-scale surface irregularities induced by energetic carbon bombardment at grazing incidence is reported. The MD simulations of energetic carbon deposition were performed with various incidence angles ranging from 0° to 70°. In the initial stage of deposition, an atomic scale surface irregularity due to the energetic carbon incidence was observed regardless of the incidence angle. However, the irregularity was saturated or diminished under normal incidence conditions, while the irregularity evolved into a large seed structure, which can provide the shadowing effect under grazing incidence conditions. The bifurcation of the growth behavior is discussed in terms of the impact-induced atomic transport on the surface: uphill transport is dominant under grazing incidence conditions, which promotes the build-up of the initial surface irregularities. However, downhill transport prevails under normal incidence conditions, which suppresses the seed structure evolution resulting in smooth surface.

2. Simulation method

Classical MD simulation method was used to study the microscopic process of a-C film growth using the reactive empirical bond order (REBO) potential developed by Brenner et al. [21]. This potential can be expressed in the pairwise dispersion-repulsion form,

$$U = \sum_i \sum_{j>i} \left[V^R(r_{ij}) - b_{ij} V^A(r_{ij}) \right]. \quad (1)$$

Here, the two terms V^R and V^A represent repulsive and attractive interactions for the pair of atoms i and j in the system, respectively. The many-body interactions due to the immediate local atomic configuration are implicitly taken into account through the bond-order function b_{ij}. This function contains dihedral angle interactions and offers smooth covalent bond formation or breaking. Specific analytic formula and parameterizations can be found in Ref. [21]. An increased C–C cutoff scheme (0.225 nm) was employed, which can avoid some unusual bonding configurations associated with the exclusively short-range character of the original cutoff settings [15,16]. The REBO potential can describe the chemical interactions between hydrocarbon atoms well, and thus has been commonly used in recent studies of nanoscale dynamic processes, (e.g., tribology [22,23] and sonomechanics [24]). The REBO potential was also benchmarked by comparing some properties of diamond such as the carbon–carbon distance, cohesive energy, elastic constants, and vacancy formation energy with the experimental results or *ab initio* density functional theory (DFT) calculations (Table 1). The implemented potential for this work was in good agreement with either the experimental data or the DFT calculations.

A diamond (0 0 1) slab served as a substrate, and its dimensions were 3.93 nm × 3.93 nm × 3.57 nm, which constituted 41 monolayers with 242 atoms in each layer (the total number of atoms was $N = 9922$). The substrate was divided into a set of layers from the bottom: the fixed layer, the heat-bath layer, and the free layer. The atoms belonging to the fixed layer, i.e., the bottom four monolayers (0.35 nm-thick) were held fixed to their equilibrium positions to mimic a semi-infinite bulk. Above the fixed layer, 17 monolayers (1.52 nm-thick) served as a heat bath layer, which equilibrated the system to room temperature, $T = 300$ K, with a Berendsen thermostat [27]. The remaining 20 monolayers (1.70 nm-thick) were considered to be a free layer in which atoms were free to evolve with full dynamics. The free layer included the open surface along the z-direction (assumed macroscopically surface normal) and had sufficient depth not to deteriorate the heat bath layer with possible implantations. The deposition of energetic carbon atoms was simulated using constant *NVE* (microcanonical ensemble) integration implemented in the large-scale atomic/molecular massively parallel simulator (LAMMPS) code [28]. Periodic boundary conditions were applied along the lateral *xy* dimensions.

The effects of the deposition angle were examined under four different incidence angles, $\theta = 0°$, 30°, 60°, and 70°, with a fixed energy of ions of $E = 75$ eV. The energy wap chosen for the access of both smoothening under normal incidence [19] and roughening under grazing incidence [4,5]. The in-plane angle of incidence wap zero (parallel with *x*-axis) in all cases. A time-step of 0.25 fs was used for the integration. The time interval between consecutive depositions was set to 4.25 ps. Prior to each deposition, the temperature of the substrate was rescaled to 300 K after the system energy fluctuation caused by the previous bombardment of energetic carbon atom had settled down. The potential energy and the root-mean-squared displacement of the atoms nearly leveled off after 3 ps from an energetic carbon incidence. Further reaction is hardly expected after the leveling-off at room temperature. Therefore, the present simulation would reproduce the growth behavior at 300 K, even if the present simulation corresponds to an unrealistically high flux of $\approx 10^{24}$ cm^{-2} s^{-1}.

3. Results and discussion

The morphology evolution as a function of the impact angle is summarized in Fig. 1. An amorphous layer was formed on the crystalline diamond substrate in all cases. The color of the

Table 1 – The bonding distance, cohesive energy, elastic constants, and vacancy formation energy of diamond calculated from the REBO potential in this work, and the comparison with those values according to the experiments or DFT calculations [25,26]

Property	This work	Expt./DFT*
r_{CC} (Å)	1.544	1.544
E_{coh} (eV)	7.37	7.37
C_{11} (GPa)	1072	1079
C_{12} (GPa)	123	124
C_{44} (GPa)	718	578
E_{vac} (eV)	7.2	7.2*

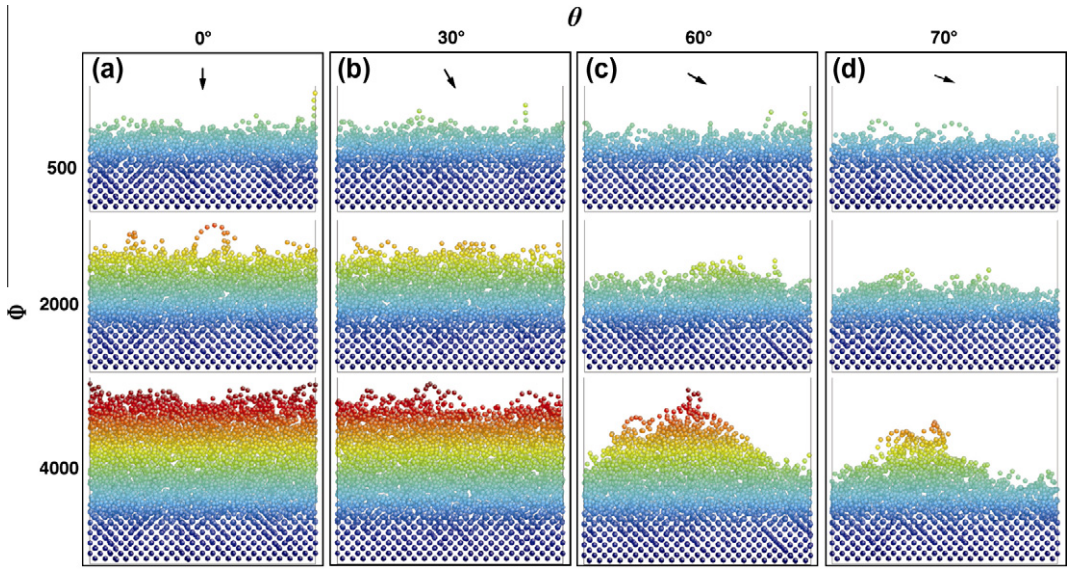

Fig. 1 – Cross-sectional snapshots of the growing film after 500, 2000, and 4000 C impacts with 75 eV of kinetic energy under incidence angles of $\theta = 0°$ (a), 30° (b), 60° (c), and 70° (d). The color encodes the height of the atoms. The arrows in the figures indicate the projection direction of incident carbon atoms in the *xz* plane. (For interpretation of the references to color in this figure legend, the reader is referred to the web version of this article.)

atoms encodes the height of the atoms. Deposition behavior of carbon is dependent on the incidence angle. Deposition yield, defined by number of deposited carbon atom per carbon incidence, decreased from 0.93 to 0.25 as θ increased from 0° to 70°, as characterized with the first 250 carbon incidences. Under the grazing incidence condition, significant amount of sputtering of surface carbon occurs resulting in much thinner film than that obtained under normal incidence condition. At normal or near-normal incidence ($\theta = 0°$, 30°), the growing surface was featureless or smooth over the course of the deposition process (Fig. 1a and b), in spite of the temporary irregularity of the surface at the atomic scale. However, at grazing incidences ($\theta = 60°$, 70°), a seed structure started to form at a carbon dose of approximately $\Phi = 2000$. Then, a bump structure was developed at $\Phi = 4000$ (Fig. 1c and d). To consider the effect of the boundary conditions of the simulation, the simulation at $\theta = 60°$ was repeated on a larger substrate of 12 nm × 12 nm × 9 nm (larger in area by a factor of approximately nine). Fig. 2 shows the surface structure that evolved on the larger substrate, which essentially exhibits the same features as in Fig. 1(c). The surface bump was evolved in any position where the seed structure was formed. However, it appeared that the surface bumps align perpendicular to the projection of incoming ions. The lateral arrangement of the bump would be understood in the analogy to the surface rippling in self-organized manner [29]. A carbon chain on the surface was temporarily observed during the deposition process. The 1-D chain or 2-D ring surface structure was reported in the MD simulations of low energy carbon deposition [30,31]. The present observation would be come up with adsorption of low-energy recoil atoms caused by ion impacts.

Fig. 3 shows that the shadowing effect on the film growth became significant at grazing incidence, while uniform deposition occurred at normal incidence. To view the evolution of the surface profile in one glance, the cross sections of the a-C film are shown, where the atoms are colored according to their entry order; blue-to-red corresponds to oldest-to-the latest (Fig. 3). Under normal incidence at $\Phi = 4000$ (Fig. 3a), the film uniformly grew in normal direction. However, a bump was clearly produced under the grazing incidence ($\theta = 70°$) at $\Phi = 5500$ (Fig. 3b) due to inhomogeneous growth toward the

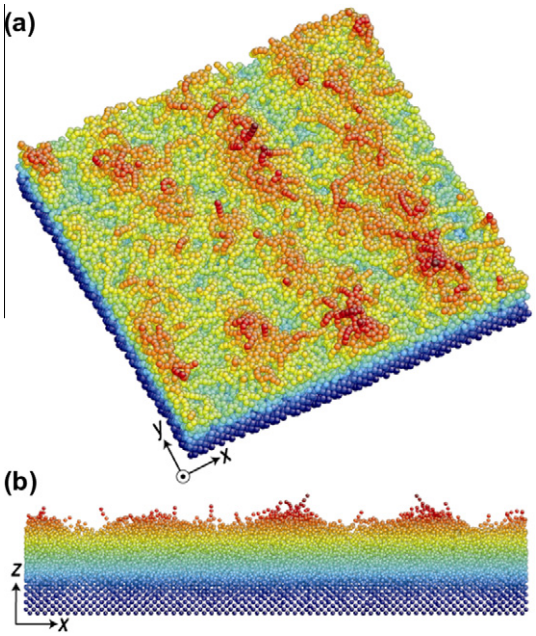

Fig. 2 – A flying view of the surface after 36,000 C impacts (a) and its side view in the *xz* plane (b). The color scheme is same as in Fig. 1. (For interpretation of the references to color in this figure legend, the reader is referred to the web version of this article.)

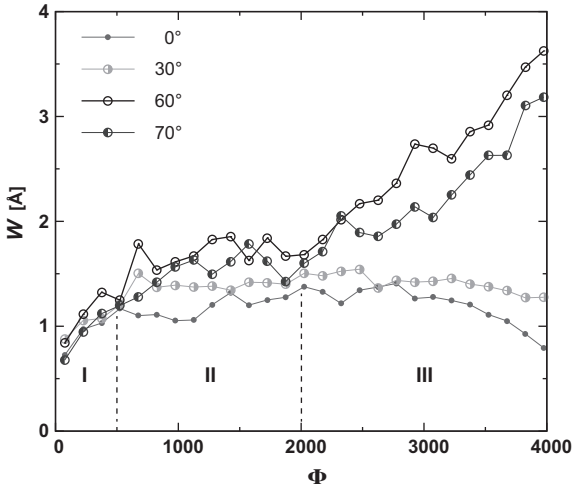

Fig. 4 – Surface roughness evolution as a function of ion dose. Note the transition from a smooth surface under near-normal incidences (0°, 30°) to a rough surface under grazing incidences (60°, 70°). The growth behavior as a function of θ branches at $\Phi = 2000$ (≈1 nm-thick) due to the shadowing effect. Thus, three stages of roughness evolution are shown: the initial roughening stage (I), the seed-forming stage (II), and the shadowing-driven rapid roughening stage (III).

beam source. The growth mainly occurred along the illuminated side of the seed structure on the surface and persisted throughout the growing process. The growth direction slightly deviated from the beam direction, which is consistent with the typical tilting behavior of nanocolumnar structures in GLAD [6]. The initial shadowing effect is operative even for a thickness of 1 nm.

The growth behavior is clearly captured in terms of the time evolution of surface roughness. Fig. 4 shows the root-mean-square surface roughness (W) as a function of Φ. The roughness is calculated from the equi-potential energy profile on the surface obtained by scanning the surface with a virtual single atom, which mimics an atomic force microscope. Long range Lennard–Jones 6–12 potential was used to calculate the potential energy between the virtual atom and the surface. The roughness evolution can be categorized in three stages: The first stage, denoted as I in the figure, is the initial roughening stage in which surfaces are roughened by initial ion impacts. All of the surfaces are roughened in a similar manner, regardless of the incidence angle, until Φ is increased to 500. This stage is an intermittent stage in which initially uniform and smooth surfaces fluctuate in height due to random impacts of energetic carbon. Surface amorphization and intermixing also occurs during this stage. The second stage is an intermediate stage, denoted as II in the figure, before the different growth modes branch out according to incidence angles. In this stage, the seed structure or the bump (see

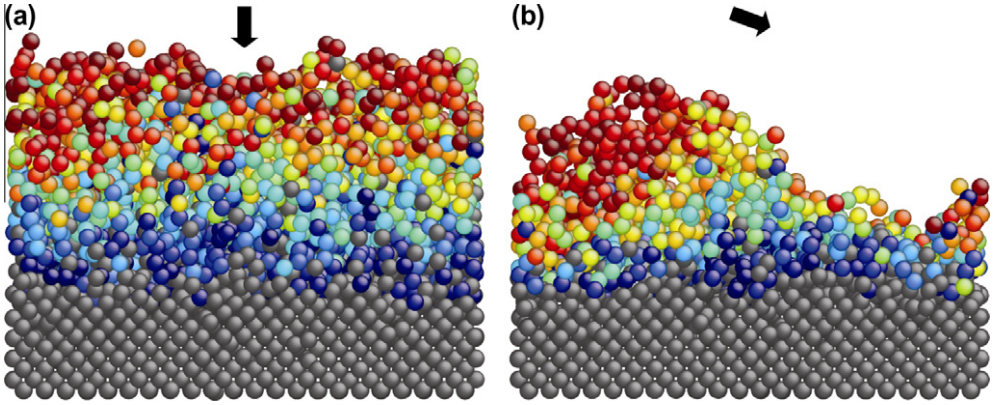

Fig. 3 – The comparison of the cross-sections of a-C film under normal (a) and grazing incidence at an angle of 70° (b). The color of the deposited atoms encodes the order of atom entry; the later atoms range from blue to red, and the original substrate is grey. The solid arrow indicates the incident ion direction. (For interpretation of the references to color in this figure legend, the reader is referred to the web version of this article.)

Fig. 1c or d) starts to form under grazing incidence ($\theta = 60°$ or 70°). However, only a slight difference in the surface roughness is observed depending on the incidence angle. As the dose increases, the third stage, denoted as III in the figure, is encountered, starting from approximately $\Phi = 2000$ (≈1 nm-thick). The growth mode clearly bifurcated according to the incidence angle. The surface roughness was saturated to a value of approximately 1 Å at normal ($\theta = 0°$) or near-normal incidence ($\theta = 30°$), which is consistent with previous experimental results on the high surface smoothness of DLC films [32,33]. In contrast, rapid roughening occurred under grazing incidence. This contrasting behavior implies that the underlying growth mechanism differed according to the incidence angle.

The origin of the two different growth modes depending on the incidence angle is discussed below. The main difference triggered by the incidence angle is the presence of persistent growth from the atomic scale surface irregularities, as shown in Fig. 3. At the grazing incidences, the surface irregularities at the early stage of the growth are sustained against further impacts to form a seed structure on the surface for the shadowing effect. Further film growth then occurs preferentially on the illuminated side of the seed structure. In the initial bump-priming stage ($\Phi = 500$–2000), the evolution of the seed structure might not be driven by the shadowing effect because the surface is still smooth at the atomic-scale ($W < 2$ Å). However, a momentum transfer from the energetic incident atoms would induce the atomic displacement on the surface, which eventually governs the evolution of the surface structure. This idea was applied to explain the smooth surface evolution in amorphous carbon growth [19]. They showed that impact-induced downhill transport at normal or near-normal incidences led initially sinusoidal surfaces or bumps to become smooth due to energetic ion deposition ($E = 30$–100 eV).

The effect of impact-induced transport was investigated by calculating the net atomic displacement vector δ after the incidence of 250 carbon atoms, where a nominally flat surface was maintained (see Fig. 4). All atoms in the sample ($i = 1 \ldots N$) were inspected for the displacement $d^{(i)}$ by the energetic carbon incidence at a dose Φ: $d^{(i)}(\Phi) = r^{(i)}(\Phi) - r^{(i)}(\Phi - 1)$. The net atomic displacement vector at Φ is thus given by $\delta_\Phi = \sum_i^N d^{(i)}(\Phi)$. The net atomic displacement vector $\delta = \sum_{\Phi=1}^{250} \delta_\Phi$ was then obtained by the consecutive impacts of 250 carbon atoms. Fig. 5(a) shows the results projected on the *xz* plane for various values of the incidence angle. The projected value of δ onto the *y*-axis is relatively small compared to the other components and, thus not shown here. The incidence angle dependence on the impact-induced transport in the *xz* plane is evident. At normal incidence, the direction of δ illustrates that the transport occurred mainly along the growth direction (+*z*), which represents some atomic intermixing in the normal direction. Net atomic transport in the lateral direction was very small. However, as the incidence angle increased, δ tilted more toward the projection direction (+*x*), which demonstrated that the lateral transport of the atoms became more significant.

The atomic displacement toward the projected incidence direction can induce uphill mass transport during deposition, which enables the initial surface irregularity to grow and provide the shadowing effect. Fig. 5b–d shows schematically the atomic displacement phenomena locally occurring on the surface with the surface irregularity evolution. The figures show the cases when the carbon with macroscopic incidence angles of $\theta = 0°$ (Fig. 5b), 50° (Fig. 5c), and 70° (Fig. 5d) are irradiated on the surface irregularities with a surface slope of $\eta = 0°$, 30°, and 60°. If the surface irregularities evolved by the initial carbon incidence, the local incidence angles vary with the slope. For a local incidence angle, δ was estimated by linear interpolation using the results of Fig. 5a. When $\theta = 0°$, δ always indicates the downhill direction on the sloped surfaces ($\eta = 30°$, 60°), as shown in Fig. 5b, which results in surface smoothening. However, drastically different behavior occurs under grazing incidence. For example, at $\theta = 50°$

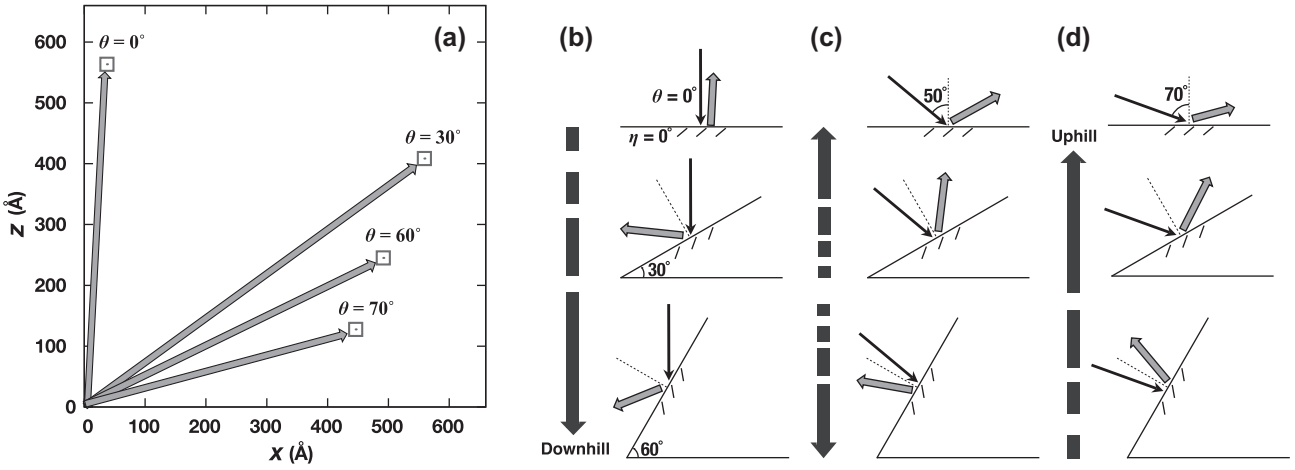

Fig. 5 – Net displacement vector δ in the *xz* plane under four different angles of incidence (a) and its implication on inclined surfaces with slopes of $\eta = 0°$, 30°, and 60° (b–d). For incidence angles other than those in (a), δ was estimated by linear interpolation. The grey arrows indicate δ (a–d), and the black arrows in (b–d) are the projection direction of the incident carbon atoms. The angle dependence of the net displacement vector can cause uphill transport along the sloped surfaces at a grazing incidence, whereas downhill transport is dominant at normal incidence (thick, dotted arrows).

(see Fig. 5c), uphill transport occurs if the slope of the surface irregularity (η) is less than the macroscopic incidence angle (θ); otherwise downhill transport is expected. There is thus competition between downhill transport and uphill transport, which is determined by the local incidence angle. At $\theta = 70°$ (see Fig. 5d), δ indicates the uphill direction when $\eta < 70°$. Therefore, up-hill transport will occur along with most sloped surfaces, amplifying the initial surface irregularities. Once a seed structure sufficient to provide the shadowing effect is created on the surface, the rough surface evolves with the proceeding carbon deposition, as shown in Fig. 3 or in stage III of Fig. 4.

4. Conclusion

Molecular dynamics simulation of the early stage of the amorphous carbon growth with various incidence angles showed that the origin of the rough surface growth under grazing incidences is mediated by the impact-induced uphill transport of the surface atoms. The atomic-scale surface irregularities in the initial stage could grow under grazing incidences because the probability of the up-hill transport of surface atoms was higher for various local incidence angles between the carbon incidence and the sloped surface irregularities. Once the seed structure developed due to up-hill transport, the shadowing effect of the seed structure resulted in rapid roughening of the surface. This mechanism could be utilized to optimize the surface structure of carbon for various applications like catalyst support or anode for secondary battery where the surface area per unit volume is to be systematically engineered.

Acknowledgements

Technical assistance from Dr. Sang-Pil Kim for the numerical evaluation of the surface roughness is gratefully acknowledged. The present work was financially supported by the KIST research program (2E22200) and by the Converging Research Center Program through the Ministry of Education, Science and Technology (2010K000992). The computation was performed using the Grand Cluster Supercomputer at KIST.

REFERENCES

[1] Kiema GK, Brett MJ. Electrochemical characterization of carbon films with porous microstructures. J Electrochem Soc 2003;150:E342–7.
[2] Simon P, Gogotsi Y. Materials for electrochemical capacitors. Nat Mater 2008;7:845–54.
[3] Yushin G, Dash R, Jagiello J, Fischer JE, Gogotsi Y. Carbide-derived carbons: effect of pore size on hydrogen uptake and heat of adsorption. Adv Funct Mater 2006;16(17):2288–93.
[4] Liu DP, Benstetter G, Lodermeier E, Vancea J. Influence of the incident angle of energetic carbon ions on the properties of tetrahedral amorphous carbon (ta-C) films. J Vac Sci Technol A 2003;21:1665–70.
[5] Lifshitz Y, Edrei R, Hoffman A, Grossman E, Lempert G, Berthold J, et al. Surface roughness evolution and growth mechanism of carbon films from hyperthermal species. Diamond Relat Mater 2007;16:1771–6.
[6] Hawkeye MM, Brett MJ. Glancing angle deposition: fabrication, properties, and applications of micro- and nanostructured thin films. J Vac Sci Technol A 2007;25:1317–35.
[7] Zhao YP, Ye DX, Wang GC, Lu TM. Designing nanostructures by glancing angle deposition. Proc SPIE 2003;5219:59–73.
[8] Vick D, Tsui YY, Brett MJ, Fedosejevs R. Production of porous carbon thin films by pulsed laser deposition. Thin Solid Films 1999;350:49–52.
[9] Janmohamed R, Steele JJ, Scurtescu C, Tsui Y. Study of porous carbon thin films produced by pulsed laser deposition. Appl Surf Sci 2007;253:7964–8.
[10] Robbie K, Brett MJ. Sculptured thin films and glancing angle deposition: growth mechanics and applications. J Vac Sci Technol A 1997;15:1460–5.
[11] Brett MJ, Hawkeye MM. Materials science – new materials at a glance. Science 2008;319:1192–3.
[12] Kaukonen HP, Nieminen RM. Molecular-dynamics simulation of the growth of diamond-like films by energetic carbon-atom beams. Phys Rev Lett 1992;68:620–3.
[13] Uhlmann S, Frauenheim T, Lifshitz Y. Molecular-dynamics study of the fundamental processes involved in subplantation of diamond-like carbon. Phys Rev Lett 1998;81:641–4.
[14] Zhang S, Johnson HT, Wagner GJ, Liu WK, Hsia KJ. Stress generation mechanisms in carbon thin films grown by ion-beam deposition. Acta Mater 2003:5211–22.
[15] Jäger HU, Albe K. Molecular-dynamics simulations of steady-state growth of ion-deposited tetrahedral amorphous carbon films. J Appl Phys 2000;88:1129–35.
[16] Jäger HU, Belov AY. ta-C deposition simulations: film properties and time-resolved dynamics of film formation. Phys Rev B 2003;68:0242011–3.
[17] Lee S, Lee C, Lee S, Lee K. Structural properties of amorphous carbon films by molecular dynamics simulation. Surf Coat Technol 2004;177–178:812–7.
[18] Ma T, Hu YZ, Wang H, Li X. Microstructural and stress properties of ultrathin diamond-like carbon films during growth: molecular dynamics simulations. Phys Rev B 2007;75:1–8.
[19] Moseler M, Gumbsch P, Casiraghi C, Ferrari AC, Robertson J. The ultrasmoothness of diamond-like carbon surfaces. Science 2005;309:1545–8.
[20] Ma TB, Hu YZ, Wang H, Li X. Effect of impact angle and substrate roughness on growth of diamond like carbon films. J Appl Phys 2007;101(1):0149011–5.
[21] Brenner DW, Shenderova OA, Harrison JA, Stuart SJ, Ni B, Sinnott SB. A second-generation reactive empirical bond order (REBO) potential energy expression for hydrocarbons. J Phys: Condens Mater 2002;14:783–802.
[22] Mo YF, Turner KT, Szlufarska I. Friction laws at the nanoscale. Nature 2009;457:1116–9.
[23] Pastewka L, Moser S, Gumbsch P, Moseler M. Anisotropic mechanical amorphization drives wear in diamond. Nat Mater 2010;10:34–8.
[24] Chew HB, Moon MW, Lee KR, Kim KS. Compressive dynamic scission of carbon nanotubes under sonication: fracture by atomic ejection. Proc R Soc London Ser A 2010;467:1270–89.
[25] McSkimin HJ, Andreatch Jr P. Elastic moduli of diamond as a function of pressure and temperature. J Appl Phys 1972;43:2944–8.
[26] Bernholc J, Antonelli A, Delsole TM, Baryam Y, Pantelides ST. Mechanism of self-diffusion in diamond. Phys Rev Lett 1988;61:2689–92.

[27] Berendsen HJC, Postma JPM, van Gunsteren WF, DiNola A, Haak JR. Molecular dynamics with coupling to an external bath. J Chem Phys 1984;81:3684–90.
[28] Plimpton SJ. Fast parallel algorithms for short-range molecular dynamics. J Comp Phys 1995;117:1–19.
[29] Chan WL, Chason E. Making waves: kinetic processes controlling surface evolution during low energy ion sputtering. J Appl Phys 2007;101:121301–46.
[30] Ma TB, Hu YZ, Wang H. Formation of linear carbon chains during the initial stage of nanostructured carbon film growth. J Appl Phys 2008;104:0649041–5.
[31] Ma TB, Hu YZ, Wang H. Formation and coalescence of linear chains in growth of nanostructured sp–sp2 amorphous carbon films. Chem Phys Lett 2008;462:104–8.
[32] Shi X, Cheah LK, Shi JR, Zun S, Tay BK. On the upper limit of sp3 content in tetrahedral amorphous carbon film. J Phys: Condens Mater 1999;11:185–9.
[33] Casiraghi C, Ferrari AC, Robertson J. The smoothness of tetrahedral amorphous carbon. Diamond Relat Mater 2005;14:913–20.